

# Accelerated High Spatial Resolution Diffusion-Weighted Imaging

Benoit Scherrer, Onur Afacan, Maxime Taquet, Sanjay P. Prabhu, Ali Gholipour, and Simon K. Warfield

Computational Radiology Laboratory, Department of Radiology  
Boston Children’s Hospital, 300 Longwood Avenue, Boston, MA, 02115, USA

**Abstract.** Acquisition of a series of anisotropically oversampled acquisitions (so-called anisotropic “snapshots”) and reconstruction in the image space has recently been proposed to increase the spatial resolution in diffusion weighted imaging (DWI), providing a theoretical 8x acceleration at equal signal-to-noise ratio (SNR) compared to conventional dense k-space sampling. However, in most works, each DW image is reconstructed separately and the fact that the DW images constitute different views of the same anatomy is ignored. In addition, current approaches are limited by their inability to reconstruct a high resolution (HR) acquisition from snapshots with different subsets of diffusion gradients: an isotropic HR gradient image cannot be reconstructed if one of its anisotropic snapshots is missing, for example due to intra-scan motion, even if other snapshots for this gradient were successfully acquired. In this work, we propose a novel multi-snapshot DWI reconstruction technique that simultaneously achieves HR reconstruction and local tissue model estimation while enabling reconstruction from snapshots containing different subsets of diffusion gradients, providing increased robustness to patient motion and potential for acceleration. Our approach is formalized as a joint probabilistic model with missing observations, from which interactions between missing snapshots, HR reconstruction and a generic tissue model naturally emerge. We evaluate our approach with synthetic simulations, simulated multi-snapshot scenario and *in vivo* multi-snapshot imaging. We show that 1) our combined approach ultimately provides both better HR reconstruction and better tissue model estimation and 2) the error in the case of missing snapshots can be quantified. Our novel multi-snapshot technique will enable improved high spatial characterization of the brain connectivity and microstructure *in vivo*.

**Keywords:** Diffusion-weighted imaging, high spatial resolution, model-based, joint model.

## 1 Introduction

Increasing the spatial resolution in diffusion-weighted magnetic resonance imaging (DW-MRI) enables substantial reduction of the intra-voxel microstructural

---

This work was supported in part by NIH grants R01 EB018988, R01 LM010033, U01 NS082320, R01 NS079788 and BCH CTREC K-to-R Merit Award.

complexity. This has been shown to enable better delineation of the trajectory of white matter (WM) fascicles [1, 11, 10] and to decrease the impact of partial voluming, critical in population studies [14] and when imaging brain structures prone to partial volume effect such as the cerebellum. However, because the SNR is directly proportional to the voxel volume, reducing the voxel size directly increases the noise of each measurement which strongly impacts the precision of estimated model parameters. High spatial resolution imaging with constant SNR can be achieved by repeating the measurements, but requires a quadratic imaging time increase. Moreover, enhancing the resolution in the slice direction requires the acquisition of additional slices to cover the same area which also increases the duration of the scans. To illustrate, reducing the resolution from  $2 \times 2 \times 2 \text{mm}^3$  to  $1 \times 1 \times 1 \text{mm}^3$  requires 128 times more imaging time at equal SNR; a 5min. acquisition would thus become a 10.7h. acquisition, which is not realistic.

Enhancing the spatial resolution requires sampling of higher frequencies in  $k$ -space which is very challenging to accomplish with high SNR and short acquisition duration time. Instead of acquiring high frequencies along all the axes simultaneously, [8] demonstrated that high-resolution (HR)  $k$ -space sampling for a diffusion gradient can be achieved by imaging this diffusion gradient with a series of anisotropically oversampled acquisitions (so-called “snapshots”) that each densely samples more frequencies along a limited number of axes (one or two). Compared to full, dense HR sampling, this multi-snapshot non-Cartesian sampling reduces the spatial encoding burden and provides substantially increased SNR for each snapshot due to the larger voxel size. In [8], an image generation model was then employed to describe how the anisotropic low resolution (LR) snapshots are observations of the unknown, underlying HR isotropic DW images we aim to recover (forward model), and the corresponding HR DW images recovered by inverting this forward model. A similar technique was later employed in [6]. A particular strength of this approach is that it only requires a conventional DW-MRI sequence and is therefore straightforward to implement. When using three orthogonal snapshots for each diffusion gradient, this effectively enhances spatial resolution along all the axes ( $x,y,z$ ) while providing an 8x theoretical reduction in imaging time compared to conventional sampling at equal SNR [8].

A major limitation in [8, 6] is that each DW image was reconstructed separately. First, the fact that the DWIs constitute different views of the same anatomy was ignored. DW images are coupled and this correlation of information can be leveraged by introducing in the reconstruction the knowledge of the local tissue microstructure. Second, an isotropic HR gradient image could not be recovered if one of its snapshots was missing, for example because of intra-scan motion, even if other snapshots for this gradient were successfully acquired.

Tobisch *et al.* [12] built upon the work in [8, 6] and proposed to introduce an ad-hoc coupling between HR reconstruction and tissue model estimation to capture the coupling between DW images. They considered the ball-and-stick tissue model at each voxel, thereby assuming 1) the presence of a single fascicle in each voxel; 2) the absence of radial diffusivity; and 3) a prefixed axial diffusivity value constant for the entire brain. This model, however, poorly represents

*in vivo* brain tissues. This is critical because, when HR reconstruction and tissue model estimation are coupled, the ability of the tissue model to accurately predict the DW signal for a diffusion gradient *conditions* the ultimate HR reconstruction accuracy. In [12], only results with synthetic simulations were reported, but no evidence of the technical efficacy of the technique was reported with *in vivo* data. More importantly, and similarly to [8, 6], this technique required the successful acquisition of *all the snapshots* for a diffusion gradient to reconstruct the corresponding HR gradient image.

In this work, we propose a novel multi-snapshot DWI reconstruction technique that simultaneously achieves HR reconstruction and tissue model estimation while enabling reconstruction with missing snapshots. Instead of an ad-hoc coupling [12], our approach is formalized as a joint probabilistic model with missing observations, from which interactions between missing snapshots, HR reconstruction and a generic tissue model naturally emerge. We describe the tissue microstructure at a voxel with a diffusion compartment imaging (DCI) tissue model that reflects the presence of tissue compartments in each voxel, providing a model-based description of the signal attenuation for any diffusion gradient orientation and strength. Our novel Simultaneous multi-snapshots High Resolution Reconstruction and Diffusion Compartment Imaging (SHORTCUT) approach enables reconstruction from snapshots with different subsets of gradients, providing increased robustness to patient motion and potential for acceleration. We evaluate SHORTCUT with synthetic simulations, simulated multi-snapshot scenario and *in vivo* multi-snapshot imaging. We investigate the robustness to missing snapshots. We show that SHORTCUT enables both better reconstruction of each DW image and better estimation of the tissue parameters.

## 2 Theory

### 2.1 The SHORTCUT Framework

We formalize SHORTCUT as a joint probabilistic model synthesized in Fig. 1. We consider  $G$  unique diffusion gradients and a maximum of  $K$  snapshots per

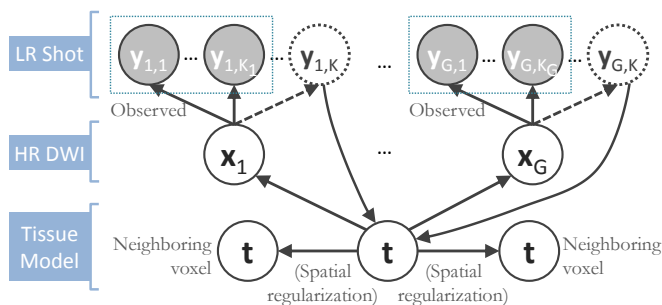


**Fig. 1.** Graphical representation of the SHORTCUT joint model in which we consider that some gradients may not be acquired in all snapshots.

gradient. We denote by  $\mathbf{y}_{g,s}$  the DW image for the snapshot  $s$  of the diffusion gradient  $g$  and by  $\mathbf{y} = (\mathbf{y}_{1,1}, \dots, \mathbf{y}_{1,K}, \dots, \mathbf{y}_{G,1}, \dots, \mathbf{y}_{G,K})$  the images of the  $KG$  snapshots in which only  $\mathbf{y} = (\mathbf{y}_{1,1}, \dots, \mathbf{y}_{1,K_1}, \dots, \mathbf{y}_{G,1}, \dots, \mathbf{y}_{G,K_G})$  have been acquired and  $(\mathbf{y}_{1,K_1+1}, \dots, \mathbf{y}_{1,K}, \dots, \mathbf{y}_{G,K_G+1}, \dots, \mathbf{y}_{G,K})$  are missing. We denote by  $\mathbf{x} = (\mathbf{x}_1, \dots, \mathbf{x}_G)$  the unknown HR DW images we aim to recover. We also consider a generic DCI tissue model dependent on some parameters  $\mathbf{t}$  that describes the DW signal attenuation at a voxel  $i$  for a diffusion gradient  $g$  by  $S_g(\mathbf{t}_i)$ . We aim at recovering **1)** the series of missing snapshots; **2)** the series of unknown HR DW images  $\mathbf{x}$ ; **3)** the parameters  $\mathbf{t}$  of the tissue model at each voxel. The simultaneous estimation of  $\mathbf{x}$ ,  $\mathbf{t}$ ,  $\mathbf{y}$  is performed according to the maximum *a posteriori* principle, by maximizing:

$$\hat{\mathbf{x}}_{\text{MAP}}, \hat{\mathbf{t}}_{\text{MAP}}, \hat{\mathbf{y}}_{\text{MAP}} = \arg \max_{\mathbf{x}, \mathbf{t}, \mathbf{y}} p(\mathbf{x}, \mathbf{t} | \mathbf{y}) = \arg \max_{\mathbf{x}, \mathbf{t}, \mathbf{y}} p(\mathbf{y} | \mathbf{x}, \mathbf{t}) p(\mathbf{x} | \mathbf{t}) p(\mathbf{t}). \quad (1)$$

**Factor**  $p(\mathbf{y} | \mathbf{x}, \mathbf{t})$ . The likelihood  $p(\mathbf{y} | \mathbf{x}, \mathbf{t})$  describes the probability of observing the snapshots  $\mathbf{y}$  given a realization of  $\mathbf{x}$  and  $\mathbf{t}$  and relates to HR reconstruction. Assuming conditional independence we can show that:

$$p(\mathbf{y} | \mathbf{x}, \mathbf{t}) \propto \prod_{g=1}^G \prod_{k=1}^{K_g} p(\mathbf{y}_{g,k} | \mathbf{x}_g, \mathbf{t}) \prod_{k=K_g+1}^K p(\mathbf{y}_{g,k} | \mathbf{t}, \mathbf{x}_g).$$

For *acquired* DW images (i.e.,  $k \in [1, K_g]$ ), we consider that all the information about  $\mathbf{y}_{g,k}$  is contained in the HR image  $\mathbf{x}_g$ . The term  $p(\mathbf{y}_{g,k} | \mathbf{x}_g, \mathbf{t})$  then describes how each snapshot constitutes an observation of the unknown  $\mathbf{x}$ . Similarly to [8], we consider an *image generation model* that describes how the LR snapshots are obtained from the unknown underlying HR volumes. Specifically, for each diffusion gradient  $g$ , we consider that  $\mathbf{x}_g$  goes through geometric and signal modifying operations to generate the  $K$  acquired LR volume:  $\mathbf{y}_{g,k} = \mathbf{W}_{g,k} \mathbf{x}_g + \epsilon_{g,k}$ , where  $\mathbf{y}_{g,k}$  and  $\mathbf{x}_{g,k}$  are expressed as column vectors by a lexicographical reordering of the pixels. We consider  $\mathbf{W}_{g,k} = \mathbf{D}_{g,k} \mathbf{B}_{g,k} \mathbf{M}_{g,k}$  where  $\mathbf{D}_{g,k}$  is the down-sampling matrix,  $\mathbf{M}_{g,k}$  is the warping matrix that maps the HR volume  $\mathbf{x}$  to the LR volume  $\mathbf{y}_{g,k}$ ,  $\mathbf{B}_{g,k}$  describes the point spread function (PSF) of the MRI signal acquisition process and  $\epsilon_{g,k}$  is the vector of residual noise. We assume that, conditionally on  $\mathbf{x}$ , the LR data  $\mathbf{y}$  are normally distributed around the unknown HR intensities with variance  $\sigma_A^2$ , so that:

$$\forall k \leq K_g, p(\mathbf{y}_{g,k} | \mathbf{x}_g, \mathbf{t}) = \frac{1}{\sigma_A \sqrt{2\pi}} \exp \left( -\frac{\|\mathbf{y}_{g,k} - \mathbf{W}_{g,k} \mathbf{x}_g\|^2}{2\sigma_A^2} \right). \quad (2)$$

For *non-acquired* images (i.e.,  $k \in [K_g+1, K]$ ) the term  $p(\mathbf{y}_{g,k} | \mathbf{t}, \mathbf{x}_g)$  describes the agreement between the missing snapshot  $\mathbf{y}_{g,k}$  and the signal arising from the DCI model for the unobserved  $k^{\text{th}}$  snapshot of the gradient  $g$ . This term relates to the missing snapshot recovery using the tissue model. We consider that all the information about  $\mathbf{y}_{g,k}$  is contained in  $\mathbf{t}$  and assume that, conditionally on  $\mathbf{y}_{g,k}$ , the intensities of the missing snapshot  $\mathbf{y}_{g,k}$  are normally distributed around the intensities of the recovered LR snapshot  $\mathbf{W}_{g,k} S_g(\mathbf{t})$  with variance  $\sigma_B^2$ :

$$\forall k > K_g, p(\mathbf{y}_{g,k} | \mathbf{t}, \mathbf{x}_g) = \frac{1}{\sigma_B \sqrt{2\pi}} \exp \left( -\frac{\|\mathbf{y}_{g,k} - \mathbf{W}_{g,k} S_g(\mathbf{t})\|^2}{2\sigma_B^2} \right) \quad (3)$$

**Factor  $p(\mathbf{x}|\mathbf{t})$ .** The term  $p(\mathbf{x}|\mathbf{t})$  describes the agreement between the series of DW images  $\mathbf{x}$  and the HR signal modeled by the tissue model and relates to the DCI model estimation. We consider that the HR image domain  $V^{\text{HR}}$  is a regular 3-dimensional (3D) grid and denote by  $\mathbf{x}_{g,i}$  the  $i^{\text{th}}$  voxel of the  $g^{\text{th}}$  HR DW image  $\mathbf{x}_g$ . We assume that, conditionally on  $\mathbf{t}$ , the HR DW images  $\mathbf{x}$  are normally distributed around the unknown modeled signal  $S_g(\mathbf{t}_i)$  with variance  $\sigma_C^2$ :

$$p(\mathbf{x}|\mathbf{t}) = \prod_{i \in V^{\text{HR}}} \prod_{g=1}^G \frac{1}{\sigma_C \sqrt{2\pi}} \exp\left(-\frac{\|\mathbf{x}_{g,i} - S_g(\mathbf{t}_i)\|^2}{2\sigma_C^2}\right). \quad (4)$$

**Factor  $p(\mathbf{t})$  :** the term  $p(\mathbf{t})$  enables us to incorporate a prior knowledge on the tissue model parameters. It can be used to introduce a regularization prior that exploits spatial homogeneity (see Section 2.3).

## 2.2 SHORTCUT-DTI and SHORTCUT-MTM.

The SHORTCUT approach derived in Section 2.1 is independent of the choice of tissue model. The simplest solution is to consider a diffusion tensor at each voxel (DTI). This amounts to modeling the signal by  $S_g(\mathbf{t}_i) = S_{0,i} \exp(-b_g \mathbf{g}_g^T \mathbf{D}_i \mathbf{g}_g)$  where  $S_{0,i}$  is the non-attenuated signal,  $\mathbf{D}_i$  is the diffusion tensor at voxel  $i$  and  $b_g$  and  $\mathbf{g}_g$  are the  $g^{\text{th}}$  b-value and unit-norm diffusion gradient direction. The parameters to estimate are  $\mathbf{t}_i = \{S_{0,i}, \mathbf{D}_i\}$  and the corresponding HR reconstruction approach referred to as SHORTCUT-DTI.

We also considered a diffusion compartment imaging model that reflects the presence of tissue compartments in each voxel and captures the non-monoexponential decay of the diffusion observed in voxels. More precisely, we considered that each compartment is in slow exchange and modeled the signal arising from each of them with a diffusion tensor. We considered in each voxel a multi-tensor model (MTM) [13] with 1) an isotropic diffusion compartment to model the diffusion of free water; and 2) a series of anisotropic cylindrical diffusion compartments to model the combined contribution of hindered and intra-axonal diffusion arising from each WM fascicle, leading to the attenuation DW signal:

$$S_g(\mathbf{t}_i) = S_0 \left[ f_{0,i} \exp(-D_{\text{iso}} b_g) + \sum_{j=1}^{N_i^f} f_{j,i} \exp(-b_g \mathbf{g}_g^T \mathbf{D}_{j,i} \mathbf{g}_g) \right], \quad (5)$$

where  $N_i^f$  is the number of WM fascicles,  $\{f_{j,i}, j = 1, \dots, N_i^f\}$  are the volumic fractions of occupancy of each compartment and sum to one,  $D_{\text{iso}}$  is the diffusivity of free water and  $\{\mathbf{D}_{j,i}, j = 1, \dots, N_i^f\}$  are tensors describing each compartment. In this case, the parameters to estimate are  $\mathbf{t}_i = \{S_{0,i}, N_i^f, (f_{j,i}, \mathbf{D}_{j,i}), j = 1, \dots, N_i^f\}$  and we refer to this HR reconstruction approach to as SHORTCUT-MTM.

## 2.3 Estimation of the model parameters.

We considered a regularization prior  $p(\mathbf{t})$  that exploits spatial homogeneity between tensors by setting  $p(\mathbf{t}) \propto \prod_{i \in V} \prod_{j=1}^{N_i^f} \exp(-\alpha_{\text{reg}} \phi(\|\nabla \log(\mathbf{D}_{j,i})\|))$  (con-

sidering  $N_i^f = 1$  for SHORTCUT-DTI), where  $\|\nabla \log(\mathbf{D}_{j,i})\|$  is the norm of the spatial gradient of  $\mathbf{D}_{j,i}$  taken in the log-euclidean space and  $\alpha_{\text{reg}}$  is a parameter controlling the regularization strength. As in [9], we chose the regularization function  $\phi(s) = \sqrt{1 + s^2/K_{\text{reg}}^2}$ ,  $K_{\text{reg}}$  being a normalization factor, to account for *anisotropic* regularization and to preserve sharp contours.

The maximization (1) was achieved by adopting a relaxation approach, by iteratively maximizing for  $\mathbf{t}$ , for  $\mathbf{y}$  and for  $\mathbf{x}$ , resulting in a novel algorithm that iteratively achieves **1)** DCI tissue model estimation; **2)** recovery of the DWIs for the unobserved snapshots; and **3)** HR reconstruction. In this work, we considered equal constant noise variances, leading to the update rules:

$$\mathbf{t}^{(n+1)} = \arg \min_{\mathbf{t}} \sum_{i \in V^{\text{HR}}} \left[ \sum_{g=1}^G \|\mathbf{x}_i^{(n)} - S_g(\mathbf{t}_i)\|^2 + \sum_{g=1}^G \sum_{k=K_g+1}^K \|\mathbf{y}_{(g,k)_i}^{(n)} - \mathbf{W}_{g,k} S_g(\mathbf{t}_i)\|^2 + \alpha_{\text{reg}} \sum_{j=1}^{N_i^f} \sqrt{1 + \|\nabla \log(\mathbf{D}_{0,i}^j)\|^2 / K_{\text{reg}}^2} \right] \quad (6)$$

$$\forall k \in [K_g + 1, K] : \mathbf{y}_{g,k}^{(n+1)} = \mathbf{W}_{g,k} S_g(\mathbf{t}^{(n+1)}) \quad (7)$$

$$\forall g \in [1, G] : \mathbf{x}_g^{(n+1)} = \arg \min_{\mathbf{x}} \sum_{k=1}^{K_g} \|\mathbf{y}_{g,k}^{(n+1)} - \mathbf{W}_{g,k} \mathbf{x}\|^2 + \|\mathbf{x} - S_g(\mathbf{t}^{(n+1)})\|^2 \quad (8)$$

This iterative algorithm is initialized by computing the mean of the observed LR snapshots. The number  $N_i^f$  of fascicle at each voxel was estimated by minimizing the generalization error [2]. We chose to estimate it only a single time after initialization of the HR reconstruction to reduce the computational burden. The steps (6), (7), (8) were achieved until the average root-mean squared difference (RMSD) between consecutive reconstructed  $\mathbf{x}^{(n-1)}$  and  $\mathbf{x}^{(n)}$  is lower than a threshold  $\theta$ . The joint HR reconstruction and tissue model reconstruction is synthesized by the pseudo-code:

```

n <- 0; Initialize each  $\mathbf{x}_g^{(n=0)}$ ,  $g = 1, \dots, G$  to the mean of the  $\mathbf{y}_{g,\cdot}$ 's
Compute  $N_i^f$  at each voxel from  $\mathbf{x}^{(0)}$  (model selection)
DO
   $\mathbf{t}^{(n+1)}$  <- Update tissue model (6)
   $\mathbf{y}^{(n+1)}$  <- Recover missing snapshots (7)
   $\mathbf{x}^{(n+1)}$  <- Update HR reconstruction (8)
  n <- n+1
WHILE  $1/K \sum_{k=1}^K \text{RMSD}(\mathbf{x}^{(n)}, \mathbf{x}^{(n-1)}) > \theta$ 
 $\mathbf{t}^{(n+1)}$  <- Update tissue model

```

### 3 Methods

**Algorithm settings.** SHORTCUT was implemented in C++. The tissue model estimation was parallelized over the image space and the DW HR reconstruction was parallelized over the space of diffusion gradients. The model-based HR reconstruction (8) was computed voxelwise by implementing the image generation model with a functional that maps a HR voxel to the LR space  $k$  accounting for downsampling, warping and sinc PSF. In SHORTCUT-MTM, the tensor representing each WM fascicle was constrained to be cylindrical. The minimizations

(8) and (6) were achieved with Broyden-CG [7], a derivative-free bound-constrained iterative algorithm that computes at each iteration a quadratic approximation for the objective function. We found that Broyden-CG provided lower cost-function minima than using a Levenberg-Marquardt scheme with estimation of the Jacobian via finite differences. The model parameters were set to  $\alpha_{\text{reg}} = 0.8$ ,  $K_{\text{reg}} = 0.01$ ,  $D_{\text{iso}} = 3 \times 10^{-3} \text{mm}^2/\text{s}$  the diffusivity of free water at  $37^\circ$  [5] and  $\theta = 0.1$ .

**Numerical phantom.** We first evaluated our approach with a numerical phantom for which a noise-free ground truth could be generated. We simulated the diffusion signal arising from 1000 tensors (FA=0.8) crossing with various angles (Fig. 2d). We considered a CUSP65 gradient encoding set [9] which achieves multiple non-zero b-values between  $1000 \text{s}/\text{mm}^2$  and  $3000 \text{s}/\text{mm}^2$  with low echo time (TE) and therefore high SNR. The DW images were corrupted with Rician noise (SNR on the  $b=0 \text{s}/\text{mm}^2$  image: 25dB). We simulated dense undersampling of  $k$ -space by removing half of the high frequencies along a single axis in Fourier space and by recovering the corresponding image in image space. This was achieved for the X, Y and Z axes and led to three orthogonal anisotropic acquisitions with a slice thickness twice the size of the in-plane resolution. We compared SHORTCUT-DTI and SHORTCUT-MTM to HR reconstruction alone (DWI with Separate high resolution reCONstruction and Diffusion model estimation, DISCORD) [8][6] by assessing the reconstruction accuracy (peak signal-to-noise ratio, PSNR) with the noise-free DW images. We also investigated the convergence of SHORTCUT and assessed the estimation accuracy of tissue model parameters for increasing number of iterations. This was achieved by comparing the compartment fractional anisotropy (cFA) of the first compartment to that of the ground truth (0.8).

**Simulated multi-snapshot scenario with *in vivo* data.** We considered an *in vivo* CUSP65 scan acquired on a Siemens 3T Trio scanner with a 32-channel head coil and the following parameters : FOV=240mm, matrix=128x128, resolution=  $1.88 \times 1.88 \times 2 \text{mm}^3$ . The Rician-noise corrected SNR in the WM measured in a  $b = 0 \text{s}/\text{mm}^2$  was  $\frac{296}{4.3} \sqrt{\frac{4-\pi}{2}} = 68.8$  (33dB). Similarly as above, we simulated three dense undersamplings of  $k$ -space by removing half of the high frequencies in Fourier space along a single axis for consecutively the axial, sagittal, and coronal orientations. We compared SHORTCUT-DTI and SHORTCUT-MTM by computing the PSNR of HR reconstructed DWIs with the original densely sampled HR DWIs (reference standard). Because the reference standard contains noise, the PSNR does not reflect the true HR reconstruction accuracy of the underlying anatomy. However, this enables investigation of the impact of the tissue model on the HR reconstruction. We compared the MTM tissue model estimated by SHORTCUT-MTM to the MTM tissue model estimated when using the original HR acquisition (HR-MTM). We assessed the relative error between the highest cFA at each voxel between SHORTCUT-MTM and HR-MTM, HR-MTM being considered as the reference standard. The maximum cFA was used as a proxy to identify at each voxel the same fascicle between the multi-tensor fields. We also compared to the relative error when estimating the MTM model after SHORTCUT-DTI reconstruction (SHORTCUT-DTI-MTM).

***In-vivo* multi-snapshot imaging.** We acquired three orthogonal CUSP65 scans on a healthy volunteer using a Siemens 3T Trio scanner with a 32-channel head coil and the following parameters : FOV=220mm, matrix=176x176, resolution= 1.25x1.25x2mm<sup>3</sup>. For each orientation, two  $b = 0\text{s/mm}^2$  images were also scanned with opposite phase encoding directions and used to correct the images for geometric and intensity distortions using *topup* (FSL). The Rician-noise corrected SNR in the WM measured in a  $b = 0\text{s/mm}^2$  was 26.4 (24.7dB). The average Rician-noise corrected SNRs in the WM for DW images at  $b = 1000\text{s/mm}^2$ ,  $b = 1500\text{s/mm}^2$ ,  $b = 2000\text{s/mm}^2$  and  $b = 3000\text{s/mm}^2$  were respectively 14.0 (19.2dB), 12.9 (18.5dB), 10.8 (17.0dB) and 9.4 (15.8dB), above SNR  $> 3$  for which the Rician distribution can be accurately approximated by a Gaussian distribution [3]. We achieved HR reconstruction and compared HR reconstruction alone (DISCORD), SHORTCUT-DTI and SHORTCUT-MTM (computational time: 20h for full brain reconstruction with a double Intel Xeon E5 processor, 8 cores each).

**Robustness to missing snapshots.** Finally, we investigated with *in vivo* data the impact of missing snapshots. We considered the aforementioned three *in vivo* CUSP65 scans and quantified the impact of discarding an increasing number  $M$  of snapshots on the estimated MTM parameters. For each number  $M \in [1, 120]$ , we randomly discarded  $M$  DW snapshots among the 195 available and computed SHORTCUT-MTM. This was repeated 100 times. We assessed the average error between the 100 estimated MTM models and the MTM estimated by SHORTCUT-MTM with full gradient sampling, considered as reference standard. This was achieved by assessing in two single fascicle regions 1) the average relative error of cFA; and 2) the average minimum angle (AMA) error [13].

## 4 Results

**Numerical phantom.** Fig. 2a shows that the RMSD between consecutive DW images reconstructions monotonically decreases toward zero, experimentally showing the convergence of the algorithm. Fig.2b shows that the average relative error of cFA gradually decreases with increasing iterations, showing the benefits of the joint SHORTCUT framework. Fig.2c shows that while SHORTCUT-DTI provides generally a higher PSNR than HR alone (DISCORD) (Fig.2c i), the over-simplistic DTI tissue model negatively impacts the reconstruction for some DW images (Fig.2c ii), particularly when the b-value is large. In contrast, SHORTCUT-MTM consistently provides the best results.

**Simulated multi-snapshot scenario with *in vivo* data.** Consistently with Fig. 2c, Fig. 3a shows that using the DTI tissue model in SHORTCUT substantially impacts the reconstruction, particularly for high b-value images. This was also verified by comparing MTM model parameters of SHORTCUT-MTM and SHORTCUT-DTI-MTM to HR-MTM over the entire white matter : the average relative error of the highest cFA at each voxel was  $0.018 \pm 7.27 \times 10^{-2}$  with SHORTCUT-MTM and  $0.031 \pm 1.35 \times 10^{-1}$  with SHORTCUT-DTI-MTM.

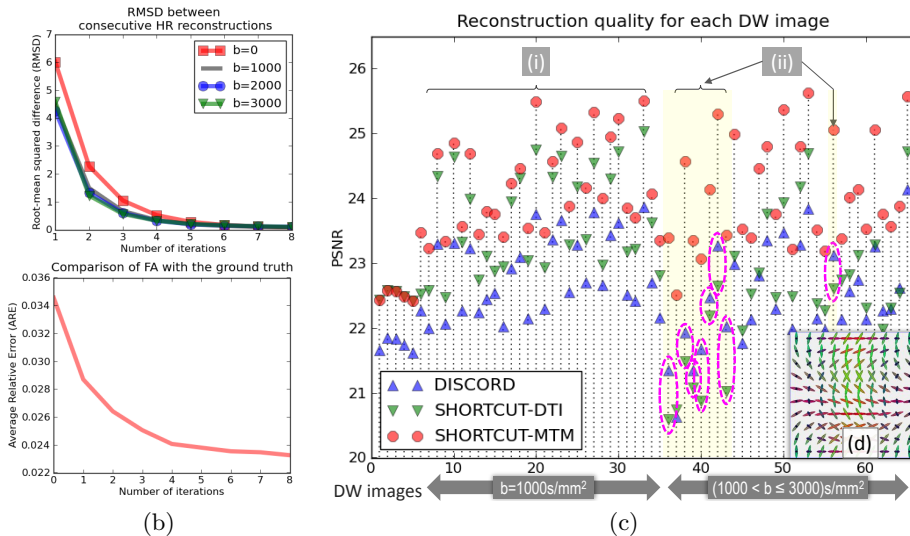


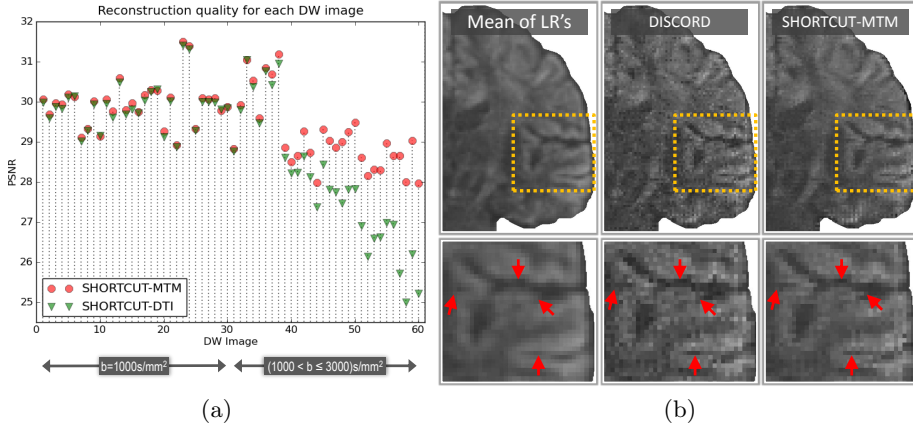
**Fig. 2.** Simulations with a synthetic phantom. (a) RMSD between consecutive DW images with SHORTCUT-MTM (for various b-value DW images). (b) Average Relative Error of the highest cFA with that of the ground truth. (c) Reconstruction accuracy for *each* DW image (PSNR). Highlighted are DWIs for which SHORTCUT-DTI provides lower PSNR than DISCORD. (d) Illustration of a slice of the numerical phantom.

***In-vivo* multi-snapshot imaging.** Fig. 3b reports the results from *in vivo* multi-snapshot imaging. It qualitatively shows that the mean of the three orthogonal snapshots for a diffusion gradient is blurred and that the HR reconstruction alone (DISCORD) is highly impacted by noise. In contrast, incorporation of the tissue model in SHORTCUT-MTM provides a regularized solution that preserves edges, qualitatively leading to a better HR reconstruction.

**Robustness to missing snapshots.** Fig. 4a shows the relative error of cFA in the cyngulum (ROI1) and in the body of the corpus callosum (ROI2). It shows that a relative error lower than 3% is ensured when a maximum of 50 gradients (i.e., 25% of the snapshots) is discarded. Fig. 4b reports the average minimum angular error. The corresponding maximum angular error is on the order of  $3^\circ$ .

## 5 Discussion

We propose a novel algorithm to achieve HR reconstruction from multi-snapshot DW imaging. Instead of performing the reconstruction of each DW image independently [8, 6], we account for the correlations between DW images by incorporating the knowledge of a local tissue model. Instead of an ad-hoc coupling [12], we formalize the simultaneous HR reconstruction and tissue model estimation with a joint probabilistic model from which interactions between the two

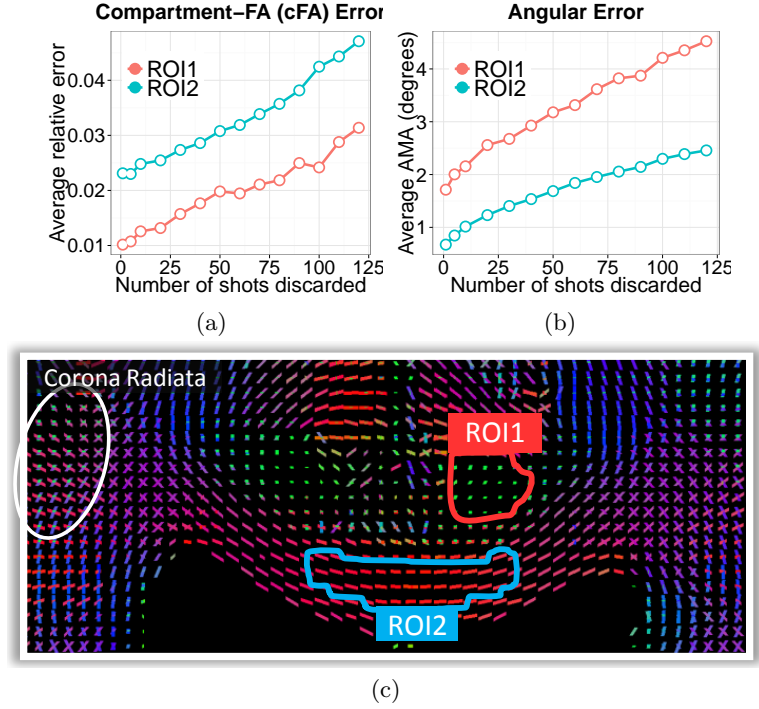


**Fig. 3.** (a) Simulated multi-snapshot scenario: impact of the tissue model on the HR reconstruction. (b) *In vivo* multi-snapshot imaging: for a  $b=1000\text{s/mm}^2$  image, qualitative evaluation of the mean of the orthogonal snapshots; the HR reconstruction alone (DISCORD); and SHORCUT-MTM. (see electronic version for better grayscale visualization).

processes naturally emerge. Importantly, and unlike [8, 6, 12], our framework enables reconstruction from snapshots with different subsets of diffusion gradients. This enables reconstruction from acquisitions in which snapshots are missing, for example due to corruption by intra-scan motion. This also provides potential for 1) scan time acceleration for a fixed gradient set or 2) increased  $q$ -space sampling for a fixed acquisition time.

We provided experimental evidence of the convergence of our novel SHORCUT algorithm (Fig.2a) and quantitatively assessed its performance (Fig.2b-c). Importantly, we demonstrated that incorporating an over-simplistic tissue model (DTI) substantially impacts the reconstruction (Fig.2c.ii, Fig.3a). This was especially observed for high  $b$ -value images, which is consistent with the known non-monoexponential decay of the DW signal for high  $b$ -values in voxels. We also showed that with *in vivo* acquisitions, HR reconstruction alone produces noisy results (Fig.3b). This is probably due to slight local misalignment of the orthogonal acquisitions caused by imperfect susceptibility distortion correction. In contrast, SHORCUT enables regularization of the reconstruction by introducing the knowledge of the local microstructure in each voxel, providing better results. Finally, we quantified the expected relative error when snapshots are not acquired (e.g., due to motion or to accelerate the acquisition) compared to full gradient sampling.

In the literature, a popular multi-shot technique is read-out segmented EPI [4] (rosEPI), which relies on the read-out of  $k$ -space with several adjacent segments and on their recombination in  $k$ -space. While rosEPI offers a slight SNR increase due to the shorter read-out of each segment (leading to lower TE),

**Fig. 4.**

Comparison of SHORTCUT-MTM with an increasing number of missing snapshots to SHORTCUT-MTM with full sampling (reference standard). Are shown the average relative error of cFA (a) and the average angular error (b) in the two single fascicle regions depicted in (c). ROI1 is selected in the cyngulum while ROI2 is selected in the body of the corpus callosum. (c) also shows that the MTM orientations matches the known orientations of WM fascicles, including three fascicles in the corona radiata.

rosEPI does not benefit from increased SNR due to the larger voxel size. Moreover, phase inconsistencies in  $k$ -space resulting from even minimal physiological motion during the application of the gradients remain challenging to correct. In contrast, our multi-snapshot high resolution technique provides, for each snapshot, a substantial SNR boost due to the larger voxel size and performs reconstruction in the image space. Similarly to rosEPI, reduced distortion can be obtained by using snapshots with low resolution in the phase encoding direction, reducing the number of phase encodes and, in the aggregate, the amount of  $T2^*$  relaxation-induced distortion.

It is important to note that, with multi-snapshot imaging and reconstruction in the image space, employing at least three *orthogonal* scans is necessary to ultimately recover high frequencies along all the dimensions. However, with only three scans, the frequencies in the corners of  $k$ -space are missing. In future work, we will evaluate the impact of this approximation by experimentally assessing the

effective spatial resolution by imaging a physical phantom. We will also evaluate the impact of 1) non-Gaussian noise modeling when using high SNR DW data (SNR on  $b = 0s/mm^2 \geq 25dB$ ); and 2) various PSF modeling strategies.

## References

1. Bach, M., Fritzsche, K.H., Stieltjes, B., Laun, F.B.: Investigation of resolution effects using a specialized diffusion tensor phantom. *Magn Reson Med* (2013)
2. Efron, B.: Estimating the error rate of a prediction rule: improvement on cross-validation. *Journal of the American Statistical Association* 78(382), 316–331 (1983)
3. Gudbjartsson, H., Patz, S.: The Rician distribution of noisy MRI data. *Magn Reson Med* 34(6), 910–914 (1995)
4. Holdsworth, S.J., Skare, S., Newbould, R.D., Guzmán, R., Blevins, N.H., Bammer, R.: Readout-segmented EPI for rapid high resolution diffusion imaging at 3T. *Eur J Radiol* 65(1), 36–46 (2008)
5. Mills, R.: Self-diffusion in normal and heavy water in the range 1-45.deg. *J. Phys. Chem.* 77(5), 685–688 (1973)
6. Poot, D.H., Jeurissen, B., Bastiaensen, Y., Veraart, J., Van Hecke, W., Parizel, P.M., Sijbers, J.: Super-resolution for multislice diffusion tensor imaging. *Magn Reson Med* 69(1), 103–113 (2013)
7. Powell, M.J.D.: The BOBYQA algorithm for bound constrained optimization without derivatives. In: Technical report NA2009/06. Department of Applied Mathematics and Theoretical Physics, Cambridge England (2009)
8. Scherrer, B., Gholipour, A., Warfield, S.K.: Super-resolution reconstruction to increase the spatial resolution of diffusion weighted images from orthogonal anisotropic acquisitions. *Med Imag Analysis* 16(7), 1465–1476 (2012)
9. Scherrer, B., Warfield, S.K.: Parametric Representation of Multiple White Matter Fascicles from Cube and Sphere Diffusion MRI. *PLoS ONE* 7(11) (2012)
10. Song, A.W., Chang, H.C., Petty, C., Guidon, A., Chen, N.K.: Improved delineation of short cortical association fibers and gray/white matter boundary using whole-brain three-dimensional diffusion tensor imaging at submillimeter spatial resolution. *Brain Connect* 4(9), 636–640 (2014)
11. Sotiropoulos, S.N., Jbabdi, S., Xu, J., Andersson, J.L., Moeller, S., Auerbach, E.J., Glasser, M.F., Hernandez, M., Sapiro, G., Jenkinson, M., Feinberg, D.A., Yacoub, E., Lenglet, C., Van Essen, D.C., Ugurbil, K., Behrens, T.E., WU-Minn HCP Consortium: Advances in diffusion MRI acquisition and processing in the Human Connectome Project. *Neuroimage* 80, 125–143 (2013)
12. Tobisch, A., Neher, P., Rowe, M., Maier-Hein, K., Zhang, H.: Model-based super-resolution of diffusion MRI. In: *Computational Diffusion MRI and Brain Connectivity Workshop*, pp. 25–34. Springer International Publishing (2014)
13. Tuch, D.S., Reese, T.G., Wiegell, M.R., Makris, N., Belliveau, J.W., Wedeen, V.J.: High angular resolution diffusion imaging reveals intravoxel white matter fiber heterogeneity. *Magn Reson Med* 48(4), 577–582 (2002)
14. Vos, S.B., Jones, D.K., Viergever, M.A., Leemans, A.: Partial volume effect as a hidden covariate in DTI analyses. *Neuroimage* 55(4), 1566–1576 (2011)